International Research Journal of Innovations in Engineering and Technology (IRJIET)

ISSN (online): 2581-3048

Volume 5, Issue 5, pp 29-34, May-2021

https://doi.org/10.47001/IRJIET/2021.505006

Development of 5 kVA Inductive Heating System

[1]Nwosu E.U, [2]Ewetumo T., [3]Arogunjo A.M, [4]Adeyemi B.

[1]PhD student, Department of Physics, The Federal University of Technology Akure, Nigeria

[2,3,4]Department of Physics, The Federal University of Technology, Akure, Nigeria

***Abstract* - An inductive heating of system (IHS) of 5 kVA has been developed for heating and melting material that their temperature is below 900°C. The IHS consist of the following units: three phase rectifier, microcontroller base varying frequency generator, MOSFET driver (IR2110), array of MOSFET bridge inverter, and inductive-capacitor resonant tank. The frequency generated can vary from 5 kHz to 1 MHz. The power supply to system was obtained from three phase rectifier and properly with high capacitance value. The MOSFET driver and MOSFET bridge inverter was connected a load comprises of inductive-capacitor resonant tank. The inductance value is 3.3 µH and capacitance value is 2.2 µF but practically obtained 2.0 µF at resonant frequency of 51.5 kHz. The result of testing and performance evaluation of the fabricated IHS carried out under open laboratory environmental condition produced were: heated iron rod to red up to 856 °C in 12 minutes at frequency of 51.5 kHz, coil current 82 A and coil voltage of 48 V; and 1.5 kg of cast Al block with Al flex was melted and temperature rise to 670°C after 42 minutes of inductive heating at frequency of 51.5 kHz, average coil current of 82 A and coil voltage of 48 V.**

Keywords: resonant tank, three phase rectification, MOSFET driver and bridge inverter.

I. Introduction

The induction heating phenomenon was first observed as an adverse heating effect produced by eddy current on the windings of electrical machines (electric motors, generators and transformers) due to alternating magnetic fields created as consequences of Lenz' and Joule's laws (Kumar and Puranik, 2016; Rudnev, *et al*, 2003; Haimbaugh, 2001; Serway and Jewett, 2010). However, the electromagnetic induction principle that drives their operations was discovered by Michael Faraday in 1837 (Laithwaite, 1991; Rudnev*et al*, 2003). After the discovery of induction principle by Michael Faraday in 1831, James C. Maxwell (1861) developed the unified theory electromagnetism of summarized as Maxwell equations which became a valuable tool in the design and analysis of modern induction heating systems. But James Joule (1840) developed the basic electrical heating law known as Joule's heating effect that helped in explaining the fundamental principle of the induction heat generation mechanism. Though the first industrial application of the IH phenomenon was proposed by Sebastian Z. de Ferranti in 1887, when he proposed IH for melting metals and filed the first patent on industrial application of IH. But, the first fully functional IH system (an induction furnace) was developed in 1891 by F.A. Kjellin. While the first major advancement in IH came in 1916 when Edwin F. Northrup implemented the first high-frequency induction furnace at Princeton. And nearly at the same time, M.G. Ribaud developed high frequency IH technology based on spark-gap generators. Also, Valentin P. Vologdin developed IH generators using machine generators and vacuum tubes which marked the beginnings of modern high-frequency induction heating systems (Lucia *et al*, 2013). The use of heating method in material (metal) processing however, only dates back to the 20th century when studies started on ways of harnessing its heat-generating properties for the purpose of melting of metals (Rudnev, *et al*, 2003). The first modern induction heating melting equipment used for steel melting was constructed in 1927 and since then, the induction heating technology have been in constant evolution following industrial and technological advances since the end of 19th century. These technological advances in induction heating were further boasted by the events of the Second World War as well as the developments in the Automotive and Aircraft industry. Which pushed application of induction heating beyond melting metals into the treatment of the metals used in the production of ammunitions and engine parts. But, in this part world (Nigeria) less work have been done on the IHS, therefore, there is need to start research into it intensively.

II. Resonant Tank Design

The result obtained from simulated using analytical and computer modeling design techniques with ANSYS Maxwell and ANSYS Multiphysics software packages (Nwosu *et. al*., 2019). The Table 1 shows the summary of requirement for the design of series resonant tank consist of inductor and bank of capacitor.

The coil inductance was calculated manually using Wheeler's formula:

$$L_{c(Wheeler's\ formula\ \}} = \frac{10\pi\mu_o N_c^2 r_c^2}{9r_c + 10l_c}(H)$$

International Research Journal of Innovations in Engineering and Technology (IRJIET)

ISSN (online): 2581-3048

Volume 5, Issue 5, pp 29-34, May-2021

https://doi.org/10.47001/IRJIET/2021.505006

$$L_{cLundi\ n'sformula} = \frac{\mu_o N^2 R^2 \pi}{l_c} k\left(\frac{2R}{l_c}\right)$$

where R is coil radius, and kis Nagaoka coefficient

The expresion for evaluation of resonant capacitance is derived from resonant frequency equation is given as:

$$C_r = \frac{1}{4\pi^2 f_o^2 L_w}$$

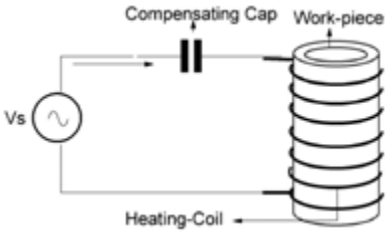

Figure 1: Series Resonant Tank

The value of capactor C_r requred is 2.2 uF series and parallel combination of 0.68 uF was to achieve 2.2 uF shown in Figure 2.

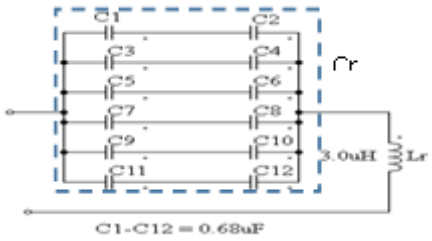

Figure 2: Schematic Diagram of the Resonant Tank Capacitor Bank Network

Table 1: Summery of the Computer model of coil-workpiece electro-thermal properties with ANSYS Maxwell and ANSYS Multiphysics software packages

S/N	Coil and Workpiece Parameters	Derived Values
1.	Coil Resistance	0.67mΩ
2.	Coil. Inductance	1.2µH
3.	Coil Impedance	0.385Ω
4.	Coil turns	7 turns
5.	Coil length	69 mm
6.	Coil excitation current	100 Amps
7.	Coil voltage	48 Volts
8.	Simulation Time	600 seconds
9.	Coil Excitation current frequency	51 kHz

III. Full-Wave Three-Phase Rectification

The uncontrolled bridge rectifier circuit for full-wave three-phase requires six diodes is obtained by using two half-wave rectifier circuits, two per phase in the same manner to the single-phase bridge rectifier. The main merit is that the circuit produces a lower ripple output than half-wave 3-phase rectifier as it has a frequency of six times the input AC waveform. The full-wave rectifier fed from a balanced 3–phase 3-wire delta connected supply as no fourth neutral (N) wire is required. The full-wave 3-phase rectifier circuit is given in Figure 3.

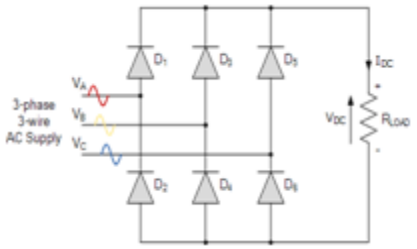

Figure 3: Full-wave Three Phase Rectifier Circuit

IV. Full-wave Three-phase Rectification Operation

The phase notation are Red-Yellow-Blue ($V_A - V_B - V_C$) and the red phase (V_A) starts at 0^o. Each phase connects between a pair of diodes as shown Figure 3. One diode of the conducting pair powers the positive (+) side of load, while the other diode powers the negative (-) side of load. Diodes D_1 D_3 D_2 and D_4 form a bridge rectifier network between phases A and B, similarly diodes D_3 D_5 D_4 and D_6 between phases B and C and D_5 D_1 D_6 and D_2 between phases C and A. Thus, diodes D_1 D_3 and D_5 feed the positive rail and depending on which one has a more positive voltage at its anode terminal conducts. Likewise, diodes D_2 D_4 and D_6 feed the negative rail and whichever diode has a more negative voltage at its cathode terminal conducts.

Then, the three-phase rectification, the diodes conduct in matching pairs giving a conduction pattern for the load current of: $D_{1\text{-}2}$ $D_{1\text{-}6}$ $D_{3\text{-}6}$ $D_{3\text{-}6}$ $D_{3\text{-}4}$ $D_{5\text{-}4}$ $D_{5\text{-}2}$ and $D_{1\text{-}2}$ as shown in Figure 4.

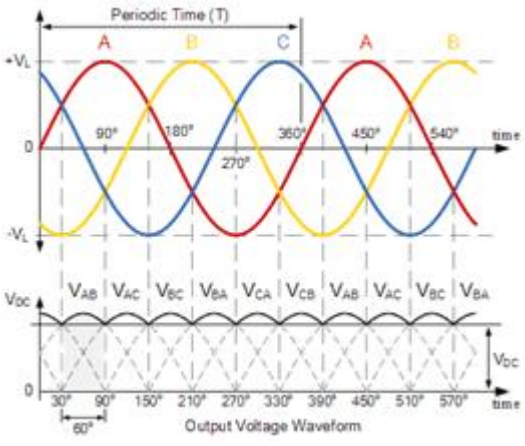

Figure 4: Output Voltage Waveform

International Research Journal of Innovations in Engineering and Technology (IRJIET)

ISSN (online): 2581-3048

Volume 5, Issue 5, pp 29-34, May-2021

https://doi.org/10.47001/IRJIET/2021.505006

V. Full-wave Three-phase Rectifier Conduction Waveform

In 3-phase power rectifiers, conduction (ON) always occurs in the most positive diode while the corresponding most negative diode is OFF. Thus, as the three phases rotate across the rectifier terminals, conduction is passed from diode to diode. Then each diode conducts for 120^o (one-third) in each supply cycle but as it takes two diodes to conduct in pairs, each pair of diodes will conduct for only 60^o (one-sixth) of a cycle at any one time as shown Figure 4.

Therefore, a 3-phase rectifier fed by "3" transformer secondaries, each phase will be separated by $360^o/3$ thus requiring 2*3 diodes. The rectifier circuit can be fed by a star connected or a delta connected transformer supply shown in Figure 5. The average DC value of the output voltage waveform from a 3-phase full-wave rectifier is given as:

$$V_{DC} = \frac{3\sqrt{3}}{\pi} V_S = 1.65 \times V_S$$

Where

$$V_S = \frac{\sqrt{2}V_{RMS}}{\sqrt{3}} \quad \text{or } V_S = \frac{V_{L(PEAK)}}{\sqrt{3}} = 1.414 \times V_{L(PEAK)},$$

V_{RMS} is root main square of line voltage and $V_{L(PEAK)}$ is the maximum line-to-line voltage.

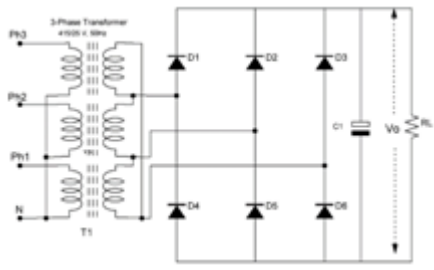

Figure 5: Three Phase Rectification with Capacitance Filter and Resistive Load

VI. Variable Square Generator using Arduino

The square-wave was generator uses the Timer One library of Arduino allows to generate a PWM signal at pin 9 in the range from about 5Hz to 1 Mhz, and duty cycle can be adjusted from 0 to 100%. The pulse generator has the ability to adjust the pulse repetition period using the buttons connected to digital inputs 6 and 7 of the Arduino. 13 input pin allows you to adjust the duty cycle. The frequency readings are displayed in LCD. The minimum step for adjusting the pulse repetition period is 1 µs, so the frequency will change discretely, for example, 1 µs is 1 MHz, 2 µs is 500 kHz, 3 µs is 333.333 Hz, and so on, and as the frequency decreases, the smoothness of its adjustment increases.

VII. Driver Circuit for MOSFET Inverter

In the driver circuit in Figure 7 used is IR2110 for the inverter circuit. The following D_1, C_1 and C_2 along with IR2110 form the bootstrap circuitry in Figure 7 for arm are D_4, C_5 and C_6. When L_{IN} is at logic 1, a signal for driving low side of MOSFET and Q_2 is ON, C_1 and C_2 get charged to the level of V_B, which is diode drop below $+V_{CC}$.

When L_{IN} is logic 0 and H_{IN} is logic 1, a signal for driving high side of MOSFET, this charge on the C_1 and C_2 is used to add the extra voltage equal to V_B above the source level of Q_1 to drive the Q_1 in high-side configuration. A large enough capacitance must be chosen for C_1 so that it can supply the charge required to keep Q_1 on for all the time.

C_1 must also not to be too large that charging is too slow and the voltage level does not rise sufficiently to keep the MOSFET on. The higher the on time, the higher the required capacitance. Thus, the lower the frequency, the higher is the required capacitance for C_1.

The higher the duty cycle, the higher is the required capacitance for C_1. The following equations are used to calculate the bootstrap capacitance.

The total charge transferred to Q_2 input capacitance from C_{BS} during T_{LON} as given given by equation 2.41 is:

$$Q_{BTotal} = Q_{GT} + [(I_{LKCs} + I_{LKGS} + I_{QBS} + I_{LK} + I_{LKDs}) \times T_{on}] + Q_{LS} \quad 2$$

where

Q_{GT} is Total gate charge; I_{LKGS} is Switch gate-source leakage current; I_{LKCS} is Bootstrap capacitor leakage current; I_{QBS} is Bootstrap circuit quiescent current; I_{LK} is Bootstrap circuit leakage current; Q_{LS} is Charge required by the internal level shifter, set as 3 nC for all HV gate drivers; T_{ON} is High−side switch on time; I_{LKDs} is Bootstrap diode leakage current.

But only I_{QBS} and Q_{GT} are the primary components of the charge supplied by the bootstrap capacitor. So other components considered negligible and are assumed to be zero (Silicon Labs, 2020). The total charge therefore approximates to:

$$Q_{BTotal} = Q_{GT} + (I_{QBS} \times T_{on}) \quad 3$$

And from the gate driver chip (IR2110) and the MOSFET (IRFB4110),

Q_{GT} = 210 nC, I_{QBS} = 230µA . $T_{LON(MIN)}$ = 1.52 µs

International Research Journal of Innovations in Engineering and Technology (IRJIET)

ISSN (online): 2581-3048

Volume 5, Issue 5, pp 29-34, May-2021

https://doi.org/10.47001/IRJIET/2021.505006

Therefore, Q_{BTotal} is 13.2 uC, hence, the bootstrap capacitance C_{BS} is evaluated by considering the bootstrap total charge (Q_{BTotal}) and the the ripple voltage ΔV_{boot} and was given by:

$$C_S = \frac{Q_{BTotal}}{\Delta V_{boot}} \qquad 4$$

The maximum allowable ripple volage ΔV_{boot} is taken as 5% of V_{DD}(Silicon Labs, 2020).

V_{DD} is Driver rated voltage equal to 12V, the boostsrap capacitance is 22 uF

The avearage gate current required to transfer the bootstrap capacitor charge at the minimum turn-on time of the low-side mosfet is then given as:

$$I_{Gav} = \frac{Q_{BTotal}}{T_{LON\ (MIN\ )}} \qquad 5$$

and the value is 831mA when $T_{LONF(MIN)}$ is 1.52 x 10^{-6} A. The minimum sink current that will discharge the low-side switch within the minimum turn-off time is:

$$I_{Gav} = \frac{Q_{BTotal}}{T_{LOF\ F\ (MIN\ )}} \qquad 6$$

is given as 501 mA when $T_{LOFF(MIN)}$ is 2.22 x 10^{-6} A. The peak peak bootstrap diode current for UF4007 is gives by:

$$I_{pk} = \frac{V_{DD} - V_D}{Rd} \qquad 7$$

is 7.5 A when V_D is 0.7 V and R_d is 2 Ω.

If an electrolytic capacitor is ued, a ceremic capacitor should be connected in parallel with this capacitor. The ceramic capacitor is not not is needed if the bootstrap capacitor is tantalium. The tantalium capacitor distingushes itself from other conventional and electrolytic capacitors in having high capacitance per volume and lower weight.

D_2 and D_3 discharged the gate capacitances of the MOSFET quickly, bypassing the gate resistors, reducing the turn-off time. R_1 and R_2 are gate current-limitting resistors. +MOSV can be up to a maximum of 500 V. $+V_{CC}$ to ground should be used for filtering. The R3, R4, R7 and R8 is gate to source resistors. They are really important on the design to prevent the burning or failing of MOSFET or damage MOSFET driver IC. Gate to source resistors prevent accidential turn ON of the MOSFET by external niose usually at startup when the gate is floating. The MOSFET may sometimes turn ON with a floating gate because of the internal drain to gate "Miller" capacitance effect. A gate to source resistors acts as a pull-down to ensure a low level for the MOSFET. The wave nature at each gate is shown on Figure 7.

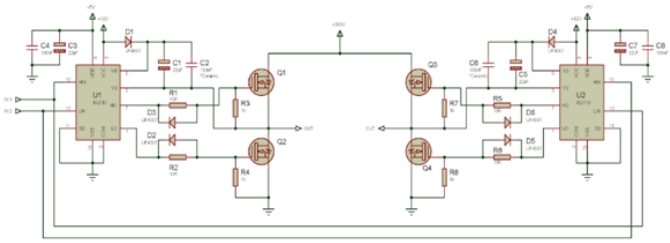

Figure 6: MOSFET Driver Circuit

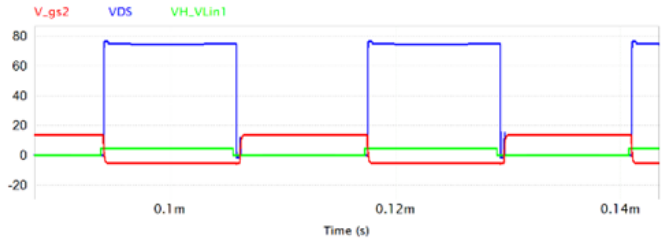

Figure 7: PSIM Simulation of the Gate Driver Circuitry output waveforms

VIII. The Inverter Circuit

The MOSFET (IRFB4110), were connected in each arm to deliver current across the load (that is the resonant tank network). The parallel connection network is on Figure 8 were used to increase current delivering to resonant tank. The single MOSFET on each arm on Figure 7 (Q1, Q2, Q3 and Q4) were replaced by Figure 9. The Figure 10 shows bottom layer view of the CSN printed circuit board (PCB) design and 3-D top layer view of the CSN (PCB component layout).

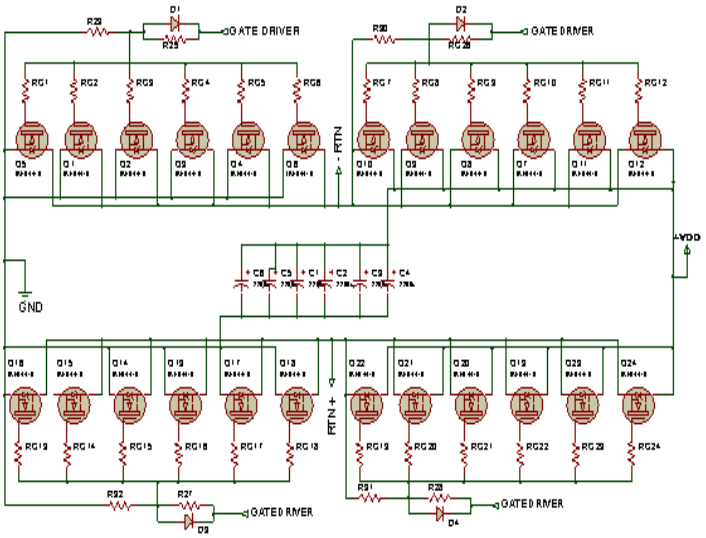

Figure 8: The Schematic Diagram of the Full Bridge Inverter Circuit with Paralleled MOSFET Transistor Connection

International Research Journal of Innovations in Engineering and Technology (IRJIET)

ISSN (online): 2581-3048

Volume 5, Issue 5, pp 29-34, May-2021

https://doi.org/10.47001/IRJIET/2021.505006

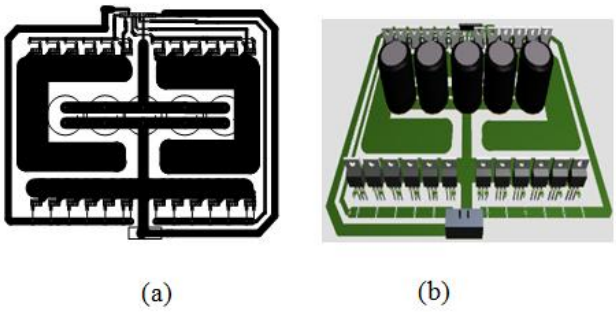

(a) (b)

Figure 9: Bottom layer View of the CSN Printed Circuit Board (PCB) Design (a) and 3-D Top Layer View of the CSN (PCB Component Layout)

IX. Result and Discussion

The system was tested by using iron crucible inside coil showing the heating and melting of the Aluminum material. The frequency was just until the current detection on the reaches maximum which is 84.21 A against initial current design of 100 A. The temperature measurement from system was given in Table 2. The Figure 10 shows pictorial progressive increase in temperature with time. The Figure 11 and 12 shows the setup and material under test. After, 600 s the Al material rises to 434^{o}C and final turn red after 42 minutes. The functionality, of the system according to result obtained from simulation by Nwosu *et al.*, 2019 expect that the current proposed by simulation was not reached. This may be due to defectiveness of active component and capacitor requirement is 2.2 uF but possible combination that can be reached by available capacitor 0.68 uF form in both series and parallel combination in Figure 3 can also, contribute for current not reached 100 A.

X. Conclusion

The testing and performance evaluation of the fabricated IHS carried out under open laboratory environmental condition produced the following results:

a. Heated iron rod to red up to 856^{o}C in 12 minutes at frequency of 51.5 kHz, coil current 82 A and coil voltage of 48 V; and
b. 1.5 kg of cast Al block with Al flex was melted and temperature rise to 670^{o}C after 42 minutes of inductive heating at frequency of 51.5 kHz, average coil current of 82 A and coil voltage of 48 V.

Generally, the heating time depended on mass of conducting materials and medium, ranging from 100s to 42 minutes. For the tested material for iron rod (17 flat and ring spanner) it took 2 minutes 30 seconds to turn red while for the cast Al block of 1.5 kg it took 42 minutes to melt and turn red.

Table 2: Workpiece Temperature after 600 seconds of heating

Time (s)	Temp (deg. C)	Voltage (Volts)	Current (Amps)	Frequency (kHz)
0	27.0			
30	47.3			
60	63.0			
90	87.2			
120	100.1			
150	139.5			
180	180.2			
210	201.5	48.0	84.21	51.1
240	233.5			
270	248.3			
300	284.0			
330	307.8			
360	325.8			
390	351.5			
420	366.8			
450	377.3			
480	388.5			
510	401.8			
540	414.0			
570	424.5			
600	434.8			

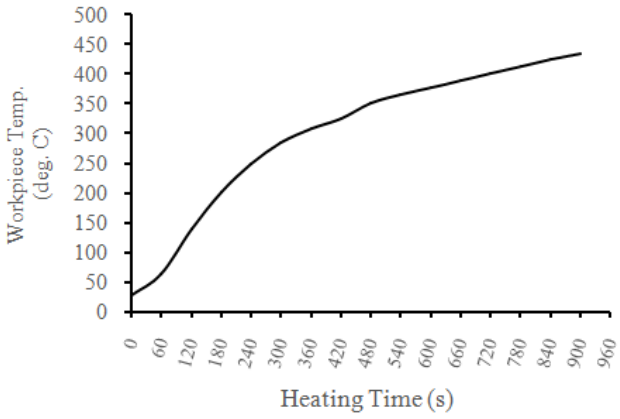

Figure 10: Graphical Plot of the Manually Measured Workpiece Temperature

Figure 11: System Experimental Setup for Testing and The LCD Display of the HIS

ISSN (online): 2581-3048
Volume 5, Issue 5, pp 29-34, May-2021
https://doi.org/10.47001/IRJIET/2021.505006

(a) (b)

Figure 12: (a) Snapshots of the Crucible inside Coil Showing (b)The Heating and Melting of The Aluminum Material

REFERENCES

[1] Kumar Shashi, C.S and PuranikD.B (2016) Induction Heating: It's Applications in Dairy Industry, International Journal of Innovative Science, Engineering & Technology, 3(03). www.ijiset.com ISSN 2348 – 7968.

[2] Rudnev Valery, Don Loveless, Raymond Cook and Micak Black (2003); Handbook of Induction heating, INDUCTOHEAT, Inc., Madison's Heights Michigan USA.

[3] Haimbaugh Richard E., (2001); Practical Induction Heat Treating, Downloaded fromwww.asminternational.org

[4] Serway Raymond A. and Jewett John W., Jr (2010), Physics for Scientists and Engineers with Modern Physics, Eighth edition, Brooks/Cole, 20 Davis Drive Belmont, CA 94002-3098, USA.

[5] Laithwaite E. R. (1991), "The influence of Michael Faraday on power engineering,"

[6] Lucia, Oscar and Maussion, Pascal and Dede, Enrique and Burdio, Jose M. (2013). Induction Heating Technology and Its Applications: Past Developments, Current Technology, and Future Challenges, IEEE Transactions on Industrial Electronics, 61(05): 2509-2520.

[7] Nwosu E.U, Ewetumo T., Arogunjo A.M, Adeyemi B. (2019), Analytical Modeling with Computer Simulation Validation of an Inductive Heating System for Metals Melting Application, ICONIC Research and Engineering Journals, IRE 1701371.

AUTHOR'S BIOGRAPHIES

NWOSU Edwin Ugochukwu, A Ph.D Student at Department of Physics, The Federal University of Technology, Akure, Nigeria.
Research option: Electronic Measurement and Instrumentation

Ewetumo Theophilus, Ph.D. Department of Physics, The Federal University of Technology, Akure, Nigeria.
Research option: Electronic Measurement and Instrumentation

Professor Arogunjo A. Muyiwa, Ph.D., Department of Physics, The Federal University of Technology, Akure, Nigeria.
Research option: Radiation and Health Physics

Professor Adeyemi Babatunde, Ph.D., Department of Physics, The Federal University of Technology, Akure, Nigeria.
Research option: Atmospheric Physics/Communication

Citation of this Article:

Nwosu E.U, Ewetumo T., Arogunjo A.M, Adeyemi B., "Development of 5 kVA Inductive Heating System" Published in *International Research Journal of Innovations in Engineering and Technology - IRJIET*, Volume 5, Issue 5, pp 29-34, May 2021. Article DOI https://doi.org/10.47001/IRJIET/2021.505006

****

